



1 **Regional difference in runoff regimes and changes in the Yarlung Zangbo river basin**

2 He Sun^{1*}, Tandong Yao^{1,2}, Fengge Su^{1,2*}, Wei Yang^{1,2}, Guifeng Huang¹, Deliang Chen³

3

4 ¹State Key Laboratory of Tibetan Plateau Earth System, Environment and Resources (TPESER),
5 Institute of Tibetan Plateau Research, Chinese Academy of Sciences, Beijing 100101, China

6 ²University of Chinese Academy of Sciences, Beijing 100101, China

7 ³Regional Climate Group, Department of Earth Sciences, University of Gothenburg,
8 Gothenburg 405 30, Sweden

9

10

11

12

13

14

15

16

17 *Corresponding author: He Sun; Fengge Su

18 State Key Laboratory of Tibetan Plateau Earth System, Resources and Environment, Institute
19 of Tibetan Plateau Research, Chinese Academy of Sciences, Beijing 100101, China

20 Email: sunhe@itpcas.ac.cn; fgsu@itpcas.ac.cn

21



22 Abstract

23 An improved understanding of runoff regimes and flow changes in the Yarlung Zangbo (YZ)
24 river basin in the southern Tibetan Plateau (TP) is crucial for water resources management.
25 However, regional characteristics in runoff regimes and changes are not comprehensively
26 investigated in the YZ mostly due to the lack of hydrometeorological observations. Here, we
27 comprehensively investigated runoff regimes and changes across six sub-basins in the YZ for
28 1971–2020 with a particular focus on the comparison between the upstream of the Nuxia (NX)
29 basin and the downstream NX-Pasighat (NX-BXK), based on a newly generated precipitation
30 dataset and a well-validated model with streamflow, glacier mass and snow cover observations.
31 Our results reveal that large regional differences in runoff regimes and changes exist in the YZ
32 basin. Firstly, runoff generation is dominated by rainfall in the entire YZ, and glacier runoff
33 plays more important role in annual total runoff (19%) in the NX-BXK than other sub-basins.
34 Secondly, annual runoff shows an increasing trend in the NX basin but a decreasing trend in the
35 NX-BXK due to rain-induced runoff changes, resulting in a weak increasing trend (3.1
36 mm/10yr) in the YZ basin. Thirdly, total runoff increases of 5%–22% in the NX but decreases
37 of 3%–20% in the NX-BXK in all seasons in 1998–2020 relative to the period 1971–1997.
38 Finally, the NX basin faces a considerably hazard from extreme flood, but the NX-BXK basin
39 faces more severe hydrological droughts. Glacier runoff shows limited roles in mitigating water
40 shortages caused by drought in dry seasons, but it intensifies the flood frequency and severity
41 among the basins in wet season. Our study offers a basic framework for clarifying the runoff



42 regimes and flow changes in the TP basins.

43

44 **Keywords**

45 Runoff Regimes, Runoff Changes, VIC-Glacier Hydrological Model, Yarlung Zangbo, Tibetan

46 Plateau

47

48 **Highlights**

49 ● A basic framework is provided to clarify runoff changes and the attribution in the TP basins.

50 ● The NX-BXK makes the largest contribution (52%) to total runoff of the YZ basin.

51 ● Annual runoff shows an increasing trend in the NX sub-basin but a decreasing trend in the

52 NX-BXK, due to opposing precipitation changes.

53 ● Glacier melt shows limited roles in mitigating water shortages caused by the drought, but

54 it intensifies flood frequency and severity in the YZ.

55

56

57

58

59

60

61



62 1 Introduction

63 The Yarlung Zangbo (YZ, Figure 1) River, also named the upper Brahmaputra, drains the
64 southern Tibetan Plateau (TP) in China. As the largest river basin of the TP, the YZ basin and
65 its two tributary (Lhasa and Nianchu river) basins serve as the main fresh water source of
66 the Tibet autonomous region (TAR), and constitute the main agricultural region in the TAR
67 (Yang et al., 1989; Zhong et al., 2014). Like elsewhere on TP, a rapid ongoing temperature rise
68 (0.3–0.4°C) may influence runoff processes and water resources availability in the YZ basin
69 (Yao et al., 2012; Li et al., 2018), and potentially increase the risk of natural hazards from floods
70 or drought in the downstream region. Therefore, a comprehensive understanding of runoff
71 regimes and flow changes in the YZ under the changing climate is crucial for decision making
72 on water resources management.

73

74 The variability of hydrological processes is high within the YZ basin with an area of about
75 250,000 km² due to the differences in climate (e.g., Indian summer monsoon and local terrain
76 effects) and physical characteristics (e.g., uneven distribution of glaciers and snow cover).
77 Many studies of runoff regimes and changes were conducted using hydrological models in the
78 YZ basin, but most simply focused on the region upstream of the Nuxia (NX) hydrological
79 station (Figure 1) (Chen et al., 2017; Cuo et al., 2019; Su et al., 2016; Zhang et al., 2013; Zhao
80 et al., 2019). Less attention was paid to the most glacierized downstream region between NX
81 and Pasighat hydrological stations (NX-BXK, Figure 1), which accounts for about 65% of total



82 glacier area in the YZ (Table 1). In addition, this region exhibits the largest glacier retreat in the
83 TP, where length has decreased at a rate of 48.2m yr^{-1} and area was reduced at a rate of 0.57%
84 yr^{-1} during the 1970s–2000s (Yang et al., 2013; Yao et al., 2012). Glacier melt can significantly
85 modify streamflow regime, including the quantity, timing, and variability of flows over space
86 and time (Barnett et al., 2005). In addition, ongoing atmospheric warming and water stress
87 makes the TP vulnerable to drought, but glaciers are a uniquely drought-resilient source of
88 water (Pritchard, 2019). Thus far, the very limited hydrological studies from the NX-BXK
89 region show contradictory results due to the use of different hydrological models, forcing data
90 and approaches. For example, Sun and Su (2020) suggested that total runoff was dominated by
91 glacier melt in the NX-BXK, but Wang et al. (2021) suggested that total runoff was dominated
92 by rain-induced runoff. Therefore, runoff regimes and changes and should be further
93 investigated in the downstream region of the YZ.

94

95 Although many hydrological studies focus on the region upstream of the NX hydrological
96 station, regional characteristics are still unclear in the basin. For example, runoff in the region
97 between Yangcun and NX hydrological stations (YC-NX) contributes of 51% to total runoff at
98 the NX hydrological station (Sun and Su, 2020); thus runoff regimes and changes in this sub-
99 basin largely affect runoff changes in the entire NX basin. In addition, runoff changes in the
100 Lhasa (LS) and Rikaze (RKZ) sub-basins, which are vital crop centers for the central Tibet
101 Autonomous Region, are crucial to irrigation water resources. Therefore, it is important to



102 investigate the runoff regimes and changes in different sub-basins of the NX, which will result
103 in improved understanding of the underlying mechanisms of runoff changes.

104

105 Existing hydrological studies show large differences in runoff regimes and changes in the NX
106 basin, which may due to variations in forcing inputs for hydrological model simulations.
107 Accurate precipitation inputs are important for reliable hydrological model simulations (Su et
108 al., 2008). However, high mountain precipitation in the YZ is still inadequately represented in
109 either gauge-based precipitation, satellite-based precipitation, reanalysis-based estimates or
110 outputs of regional climate models (Liu et al., 2020; Sun and Su, 2020; Sun et al., 2021). In
111 addition, streamflow and glacier observations are inadequate for model calibration and
112 validation, limiting simulation accuracy in the YZ basin. Most studies only validate
113 hydrological models using streamflow observations, yet realistic runoff simulations at the
114 catchment outlet cannot guarantee reasonable simulation results (Duethmann et al., 2014)
115 because of the compensation between precipitation-induced runoff and glacier runoff. To
116 address the above issues, in this study we collected precipitation observations at 280 gauges,
117 streamflow observations at eight hydrological stations, glacier mass balance observations at
118 two sites, and satellite-based glacier and snow cover area estimates in the YZ basin (Figure 1).
119 These constitute a basin-wide observation dataset enabling us to validate hydrological models,
120 and reveal runoff regimes and flow changes in the YZ basin.

121



122 Based on the basin-wide observation dataset, in this study, runoff regimes, changes, and the
123 attributions across six sub-basins in the YZ for 1971–2020 with a particular focus on the
124 comparison between the NX and NX-BXK are comprehensively investigated using the Variable
125 Infiltration Capacity (VIC)-Glacier hydrological model. Our intents are to: (1) use the model
126 framework to identify runoff regimes and changes, and quantify the contributions of three major
127 runoff components (glacier, rain-induced, and snowmelt runoff) to total runoff in the YZ and
128 its subbasins; and (2) investigate responses of runoff and the three components to climate
129 changes at annual, seasonal, and extreme flow scales. We expect these findings will provide a
130 basic framework to study cryospheric basin hydrological cycles in the TP, and provide adopting
131 strategies to water resource managers based on a solid scientific understanding. We introduce
132 several novel components which may advance our understanding of the YZ hydrology:

133 (1) The analysis uncovers spatially varying runoff regimes and changes across six sub-
134 basins of the YZ basin, associated with heterogeneous surface characteristics.

135 (2) A basin-wide observational hydrometeorology network is used to validate glacier-
136 hydrological model to quantify runoff processes under climate-cryosphere changes.

137 (3) A comprehensive long-term precipitation dataset with a high spatiotemporal resolution
138 (Sun et al., 2022) is used to improve hydrological simulations in this high-altitude basin.

139

140 **2 Study Area**

141 In this study, the entire YZ basin is divided into six sub-basins based on flow direction and



142 locations of hydrological stations (Figure 1; Table 1). There are five sub-basins in the basin
 143 upstream of the Nuxia (NX) hydrological station, also named NX basin, and a sub-basin
 144 between Nuxia and Pasighat (NX-BXK) hydrological station. The NX basin includes the
 145 upstream sub-basins of Lhatse (LZ), Shigatse (RKZ) and Lhasa (LS) hydrological stations, the
 146 sub-basin between Lhatse and Yangcun (LZ-YC) hydrological station, and the sub-basin
 147 between Yangcun and Nuxia (YC-NX) hydrological station. The climate of the YZ is
 148 characterized by a wet and warm summer and a cool and dry winter, and precipitation is mostly
 149 dominated by summer monsoon (Figure S1 in Supporting Information). In addition, mean
 150 annual precipitation increases from upstream (283 mm) to downstream (1465 mm), with a mean
 151 of about 774 mm in the entire YZ basin (Table 1). All sub-basins show similar seasonal patterns
 152 of temperature, with peaks mostly occurring in July–August (Figure S1). Glacier coverage
 153 ranges from 0.9% (LZ-YC) to 10.2% (NX-BXK), with an average of 3.3% in the entire YZ
 154 basin. The largest glacier coverage distributes in the YC-NX (2.8%) and NX-BXK (10.2%) sub-
 155 basins (Table 1). The snow cover fraction (SCF) ranges from 7% (RKZ) to 32% (NX-BXK),
 156 with an average of 19% in the YZ basin.

157

158 **3 Data and Methodology**

159 **3.1 VIC-Glacier Hydrological Model**

160 The physically based and distributed VIC hydrological model (Liang et al., 1994; Liang et al.,
 161 1996) linked with a simple degree-day glacier melt algorithm (Hock, 2003), referred to as VIC-



162 Glacier, is used in this study, which can simulate the physical exchange of water and energy
163 among soil, vegetation, and atmosphere over a grid mesh. The VIC-Glacier model has a two
164 layer energy-balance snow model (Cherkauer and Lettenmaier, 1999) and a frozen
165 soil/permafrost algorithm (Cherkauer and Lettenmaier, 1999; 2003), and has been previously
166 used in runoff simulations for several high-mountainous TP basins (Meng et al., 2019; Su et al.,
167 2016; Sun and Su, 2020; Tong et al., 2016; Zhang et al., 2013; Zhao et al., 2019).

168

169 Here, the modeling framework at a $1/12^\circ \times 1/12^\circ$ (approximately 10 km \times 10 km) spatial
170 resolution and a three-hourly time step is adopted from Sun and Su (2020). The required forcing
171 input data for the VIC-Glacier model include daily meteorological forcing data (precipitation,
172 maximum and minimum temperatures, and wind speeds) with a spatial resolution of 10 \times 10 km
173 for 1961–2020, which is adopted from Sun et al. (2022). The daily gridded estimates from the
174 newly released fifth-generation reanalysis (ERA5) precipitation of the European Centre for
175 Medium-Range Weather Forecasts was corrected based on 580 rain gauges in the monsoon-
176 dominated TP region and the machine learning algorithm (Sun et al., 2022). The developed
177 precipitation data set was evaluated at a point scale by comparing it with gauge observations,
178 and has been inversely assessed its potential utility in the VIC-Glacier hydrological simulation
179 in the YZ basin (Sun et al., 2022).

180

181 According to the source of runoff generation, total runoff is partitioned into three components



182 in this study: rain-induced runoff, snowmelt runoff, and glacier runoff. In this study, glacier
 183 runoff is defined as all water generated in the glacierized area, including rain-induced, snow
 184 melt, and ice melt in the glacierized area. The simulated total runoff from each grid cell can be
 185 calculated as

$$186 \quad R_i = f \times R_{glac} + (1 - f) \times R_{vic} \quad (1)$$

187 where, R_i is the total runoff (mm) in grid I , f is the percentage of glacier area, and glacier area
 188 is updated every year, R_{glac} is the runoff (mm) from the glacier area, and R_{vic} is the runoff
 189 (mm) calculated from the VIC model (the sum of surface runoff and baseflow) in the non-
 190 glacierized area, including both rain-induced and seasonal snowmelt runoff.

191

192 The calculated glacier area and volume are updated every year in the model by the volume-area
 193 scaling approach (Bahr et al., 1997). We use an exponential form (equation 2), derived from the
 194 glacier observation in the western China (Liu et al., 2003), to convert the glacier area to volume
 195 for a basin:

$$196 \quad V = 0.04S^{1.35} \quad (2)$$

197 where V is glacier volume and S is glacier area. The initial glacier volume is determined
 198 using glacier area from the first Glacier Inventory of China (CGI V1.0,
 199 <http://westdc.westgis.ac.cn/glacier>) dataset, and is updated every year with the snowfall
 200 accumulation and simulated ice melt from all the glacier cells. The updated glacier area is then
 201 validated by the Randolph Glacier Inventory (RGI V6.0) dataset.

202



203

204 **3.2 Model Calibration and Validation**

205 Two categories of model parameters need to be calibrated for the VIC-Glacier model: (1) the
206 degree day factor (DDF) related to glacier runoff simulation; and (2) the parameters of the VIC
207 model related to runoff simulation in non-glacierized regions, mostly including the depth of the
208 first and second soil layers (D1 and D2), the infiltration shape parameter (B_{inf}), and three base
209 flow parameters (D_s , W_s , and D_{smax}).

210

211 The VIC-Glacier hydrological model is calibrated by a systematic two-step approach. Observed
212 streamflow, observed glacier mass balance, satellite-based glacier area and snow cover fraction
213 estimates are applied to calibrate and validate the model in this study (see Table 2 for more
214 details). The Nash-Sutcliffe efficiency (NSE), relative bias (RB, %), and correlation coefficient
215 (CC), are applied to assess the performance of the hydrological model.

216

217 First, initial values of DDF parameters in the glacier model related to glacier and snowmelt are
218 adopted from Sun and Su (2020). The glacier model is calibrated to match the glacier area
219 observation from RGI V6 for 2000s–2010s, and validated by observed mass balance data from
220 Gurenhekou and Parlung No.94 glacier sites (Table 2). Based on the good performance of
221 glacier area simulation (with RB of mostly $< 7\%$, Figure 2c), the final DDF are adjusted across
222 six sub-basins (Table 1). In addition, the simulated variations in annual glacier mass balance
223 are further validated with observations at Gurenhekou Glacier for 2005–2009 and Parlung



224 No.94 Glacier for 2006–2018 in the YZ basin, which satisfactorily track the annual variations
 225 of the observed glacier mass balances, with CCs of 0.96 and 0.65, and RBs of -15% and -40%
 226 for the Gurenhekou (Figure 2a) and Parlung No.94 (Figure 2b) glaciers, respectively.
 227

228 Second, the VIC-related model parameters (mostly B_{inf} and D2) are calibrated and validated
 229 with streamflow observations at eight hydrological stations across the six sub-basins. The VIC-
 230 Glacier model captures well the magnitudes and patterns of observed runoff at daily (Figure
 231 3a), monthly (Figure S2) and seasonal (Figure 4) scales, with NSEs of 0.75 to 0.94 and RBs of
 232 -8% to 4.0% for the study basins. The closed agreements between the observed and simulated
 233 runoff are also seen at the annual scale (Figure 5), with a CC of 0.4–0.9. In order to further
 234 evaluate the model performance in simulating extreme streamflow, the flow duration curve
 235 (FDC) is used in the probability of daily runoff simulation, which represents the relationship
 236 between the magnitude and frequency of the daily streamflow in a particular river basin and
 237 provides an estimate of the percentage of time during the entire study period (Lutz et al., 2016).
 238 Here, the 95% and 5% probability of exceedance is defined as the threshold of flood and
 239 hydrological drought events. Simulated runoff can accurately capture the magnitudes of low
 240 and moderate daily observation but slightly underestimate flood prediction by less than 5% at
 241 the NX hydrological station (Figure 3b). After the careful calibration and validation, in this
 242 study, the final values of D1, D2 and B_{inf} for each grid cell are set to 0.1 m, 0.8–1.5 m, and
 243 0.2 across six sub-basins, respectively.



244 As additional validation of the model, the satellite-based SCF data are compared with the model
245 simulations for 2001–2019 in the YZ basin (Figure 6). The simulated SCF follows the monthly
246 variation of the satellite-based data with a CC of 0.60–0.82 ($p < 0.05$) and RB within $\pm 12\%$
247 among the basins, suggesting satisfactory performance of the VIC-Glacier model.

248

249 **4 Results**

250 **4.1 Runoff Composition**

251 Figure 7 shows mean monthly simulated rain-induced, snowmelt and glacier runoff, and mean
252 annual contribution of them to total runoff across six sub-basins for 1971–2020. More than 60%
253 of the annual total runoff occurs in June–September and 10%–15% in November–February in
254 the YZ and all its sub-basins for 1971–2020 (Figure 7, Figure S1). The seasonal pattern of rain-
255 induced runoff is consistent with that of total runoff. Due to co-occurrences of peak
256 precipitation and temperature in June–September, the simulated glacier runoff mostly occurs
257 during June–September for all the basins, with the peak in July and August. Snowmelt runoff
258 in the YZ and its sub-basins occurs mostly during April–October, while the peak month of
259 snowmelt differs among the sub-basins. Snowmelt runoff peaks in July–September in the LZ,
260 RKZ, LS, and LZ-YC sub-basins (Figure 7a–d), which may be due to the melting of fresh
261 snowfall in the warm season, thus helping to sustain the irrigation water supply. Snowmelt also
262 shows a peak in the downstream sub-basins (Figure 7e, f), but the peak occurs in May–June.
263 The seasonal pattern of snowmelt in the entire YZ basin is similar to that in downstream sub-



basins, with the peak in May–June.

Large differences in runoff contribution to total runoff at Pasighat outlet exist across six sub-basins of the YZ basin (Figure 7). The NX-BXK contributes 52% to total runoff at the Pasighat outlet of the YZ basin (Figure 1), followed by YC-NX (25%), LS (10%), and other sub-basins, with contributions of 3%–6%. In addition, contributions of three runoff components to total runoff are also different across six sub-basins, mostly due to heterogeneous surface characteristics. Total runoff in the YZ and all its sub-basins is dominated by rain-induced runoff, which contributes 59%–72% to annual total runoff across six sub-basins, with an averaged contribution of 62% in the entire YZ basin. Snowmelt contributes 22% to annual total runoff in the YZ basin, and 14%–36% across six sub-basins, with the largest distributed in the LS sub-basin (36%). Glacier runoff contributes 16% to annual total runoff in the YZ basin, and 5%–19% to annual total runoff across six sub-basins. The largest contribution is in the NX-BXK (19%) and YC-NX (16%) sub-basins, where there is about 78% of the YZ total glacier area.

4.2 Runoff Changes and the Attribution

In this section, based on simulated total runoff and its three components, runoff changes and their attributions in the entire YZ and its sub-basins during 1971–2020 are investigated at annual, seasonal and extreme flow scales.



284 4.2.1 Annual Scales

285 Figure 8 shows annual variations of the simulated total runoff and the three runoff components,
 286 and basin precipitation and temperature in the YZ basin during 1971–2020. Annual variations
 287 of precipitation, temperature, and simulated runoff in the sub-basins are presented in Figure
 288 S3–S7. Divergent annual runoff changes are evident among the sub-basins of the YZ. The
 289 simulated annual total runoff shows increasing trends of 8.1–18.8 mm/10yr for 1971–2020 in
 290 all sub-basins of the NX, except for the RKZ sub-basin (-1.1 mm/10yr), resulting in a
 291 significantly increasing trend of 9.4 mm/10yr ($p < 0.05$) over the entire NX basin; this is mostly
 292 due to increases in rain-induced and glacier runoff, along with significant increases in
 293 precipitation and temperature (Figure 8a). In contrast, total runoff in the NX-BXK shows a
 294 significantly decreasing trend of 9.4 mm/10yr ($p < 0.05$) for 1971–2020 (Figure 8b), resulting
 295 from a large decrease of rainfall-induced runoff (-22 mm/10yr) and seasonal snowmelt (-5.5
 296 mm/10yr) from non-glacierized areas. It is worth noting that glacier runoff exhibits a
 297 significantly increasing trend (6.0 mm/10yr, $p < 0.05$) in NX-BXK during 1971–2020, which
 298 partly compensated for the decreasing trend of total runoff in this sub-basin. As an integrated
 299 result of increased total runoff in the NX and decreased runoff in the NX-BXK, the total runoff
 300 in the entire YZ basin shows a weakly increasing trend of 3.1 mm/10yr, mostly due to increases
 301 of rain-induced and glacier runoff (Figure 8c). There is a strong correlation between annual
 302 variation of total runoff and rain-induced runoff in the YZ and all sub-basins (CC of 0.90–0.99,
 303 $p < 0.05$), while total runoff shows only weak relationships with temperature and glacier runoff



304 in the YZ and its sub-basins (Figure S8), suggesting a dominant role of rainfall-induced runoff
 305 from non-glacierized areas and minor impacts from glacier runoff on annual runoff.
 306
 307 Besides runoff changes, divergent annual variations of rain-induced, snowmelt and glacier
 308 runoff contributions for 1971–2020 are also apparent in the YZ basins (Table 3, Figure S9). The
 309 contribution of snowmelt to total runoff shows consistently decreasing trends among the basins,
 310 with significantly decreasing trends in the YZ basin ($-1.1\%/10\text{yr}$, $p<0.05$) and its NX sub-basin
 311 ($-0.5\%/10\text{yr}$, $p<0.05$). The contribution of glacier runoff decreases of $-0.1\%/10\text{yr}$ in the NX
 312 sub-basin, while it increases in the NX-BXK sub-basin ($0.8\%/10\text{yr}$), mostly due to an increase
 313 in glacier runoff and a decrease of total runoff. In contrast, the contribution of rain-induced to
 314 total runoff increases in the NX sub-basin ($1.1\%/10\text{yr}$), while it decreases in the NX-BXK sub-
 315 basin ($-0.7\%/10\text{yr}$), resulting in an increasing trend of $0.2\%/10\text{yr}$ in the entire YZ basin.
 316
 317 Cuo et al. (2019) examined the precipitation and streamflow mutations by the Mann-Kendall
 318 analysis in the YZ basin, and suggested that precipitation shows no mutation while streamflow
 319 mutates in 1997 at NX hydrological station. Based on long-term runoff observation, this abrupt
 320 change is also displayed in this study. Trends in total runoff are opposite before and after the
 321 year 1998 in the YZ and its NX and NX-BXK sub-basins, due to opposing trends in
 322 precipitation (Table 3). Annual total runoff shows increasing trends ($8.9\text{--}48.1\text{ mm}/10\text{yr}$) in the
 323 basins during 1971–1997, mostly due to an increasing trend of rain-induced runoff, seasonal



324 snowmelt and glacier runoff. However, total runoff shows insignificantly decreasing trends (-
325 0.3 to -3.3 mm/10yr) during 1998–2020. It may be attributed to a decreasing trend of rain-
326 induced by the weakening Indian monsoon after the period 1998–2000 (Liu et al., 2012; Wu
327 and Duan, 2008; Wu and Duan, 2009; Yang et al., 2014a). It is worth noting that, the decreasing
328 trend of precipitation is faster in NX-BXK (-16.0 mm/10yr) than that in NX (-7.0 mm/10yr,
329 Table 3). This difference may result from the different influences of the weakening Indian
330 monsoon during 1998–2000 (Figure S10). The NX-BXK basin is more sensitive than NX to the
331 weakening Indian monsoon during 1998–2000 (Figure S10). However, the decreasing trend of
332 total runoff is slower in NX-BXK (-0.3 mm/10yr) than that in NX (-3.3 mm/10yr, Table 3)
333 during 1998–2000, resulting from different influences of glacier runoff on total runoff between
334 NX and NX-BXK sub-basins. A faster increasing trend of glacier runoff in NX-BXK (16
335 mm/10yr), than that in NX (0.7 mm/10yr, Table 3), partly compensates for the faster decreasing
336 trend of rain-induced runoff, resulting in a slower decreasing trend of total runoff in NX-BXK.
337 Therefore, glacier runoff has been playing an increasing role in runoff changes as a result of
338 accelerated warming in the region.

339

340 **4.2.2 Seasonal Scales**

341 Changes in melt water from glaciers and seasonal snow modify total runoff regimes with respect
342 to both quantity and timing, and thus are of particular importance to water availability in warm
343 and dry seasons (Barnett et al., 2005). Relative to the period 1971–1997, divergent seasonal



344 changes in total runoff are apparent in the YZ basin during 1998–2020. For the NX basin, total
 345 runoff tends to increase by about 5%–22% in all seasons, with the largest increases appearing
 346 during May–August (11%–22%), mostly due to increases in rain-induced and glacier runoff.
 347 The smallest increases are during December–February (4.8%–5.7%), mostly due to increases
 348 in rain-induced runoff in the NX (Figure 9a, d; Table S1). Snowmelt runoff strongly increases
 349 during March–May (24%–50%) due to early snow melting (Figure 9d; Table S1), which may
 350 be beneficial to agricultural water supplies. On the contrary, total runoff decreases by about
 351 3%–20% in all seasons in the NX-BXK sub-basin (Figure 9b; Table S1) due to decreases in
 352 rain-induced runoff and seasonal snowmelt. This indicates a trend towards drier conditions,
 353 although increased glacier runoff compensates slightly for the loss of total runoff in July–
 354 August (Figure 9e). As an integrated result of seasonal changes of runoff in NX and NX-BXK,
 355 total runoff in YZ increases by 3.0%–20.0% in June–September, mostly due to increases in rain-
 356 induced and glacier runoff, while it decreases in the other months because of decreased rain-
 357 induced runoff and seasonal snowmelt (Figure 9c, f).

358

359 The distinct seasonal changes of rain-induced, snowmelt, and glacier runoff largely determine
 360 the seasonal changes of their contributions to total runoff in the entire YZ basin and its NX and
 361 NX-BXK sub-basins. Relative to 1971–1997, the rain-induced contribution increases by 5%–
 362 8% during May–October in the NX for 1998–2020, but the glacier and snowmelt contribution
 363 decreases by -0.3% to -2% and -5% to -7% in these months, respectively (Figure 9g, Table S1).



364 On the contrary, the contributions of rain-induced runoff and snowmelt decrease by -2% to -6%
 365 during May–October in the NX-BXK, but glacier contribution increases by 2%–7% in these
 366 months (Figure 9h, Table S1), showing increased importance of this season in sustaining
 367 summer water supplies in the NX-BXK. As an integrated result, for the entire YZ basin (Figure
 368 9i) glacier contribution increases by 0.5%–2% (Table S1) during June–October, and the
 369 seasonal changes of rain-induced and snowmelt contributions to total runoff are similar to that
 370 in the NX basin.

371

372 **4.2.3 Extreme Flow Scales**

373 The magnitude and timing of flow extremes tend to be altered under climate change.
 374 Contrasting extreme frequency between hydrological drought and flood days for 1971–2020
 375 exist in the YZ and its sub-basins (Figure 10). Flood frequency shows a decreasing trend of -1
 376 days/10yr for 1971–2020, but drought frequency shows an increasing trend of 3 days/10yr in
 377 the YZ basin (Figure 10c, Table S2), which could lead to the droughts of higher duration and
 378 severity. This contrast also exist in the NX and NX-BXK sub-basins (Figure 10a,b; Table S2).
 379 In addition, opposing trends occur between these two sub-basins, whether drought or flood
 380 events. Drought days shows a decreasing trend of -6 days/10yr in the NX, but an increasing
 381 trend of 6 days/10yr in the BXK (Figure 10a,b; Table S2), mostly due to opposing trends in
 382 precipitation (Figure 8). On the contrary, flood days shows an increasing trend of 6 days/10yr
 383 in the NX, but a decreasing trend of -3 days/10yr in the BXK (Figure 10a,b; Table S2). This is



384 similar to the tendency of annual maximum daily runoff (Figure 10d–f). The annual-maximum
 385 daily runoff increases in the NX, but decreases in the NX-BXK. Trends in annual-maximum
 386 daily runoff are also opposite before and after the year 1998 in the YZ and its NX and NX-BXK
 387 sub-basins, with increasing trends (0.1–0.7 mm/10yr) during 1971–1997 and decreasing trends
 388 of -0.1 to -0.5 mm/10yr during 1998–2020 (Figure 10d–f, Table S2).

389

390 As with the runoff changes described above, extreme frequency changes are mostly influenced
 391 by monsoon precipitation in the YZ basin. It is worth noting that glacier runoff plays an
 392 increasing role during 1971–2020 in both annual and summer water supplies in the YZ (Figure
 393 7–9), and it is a uniquely drought-resilient source of water in the high-mountainous regions
 394 (Pritchard, 2019). Flow duration curves for simulated daily total runoff, glacier runoff, and
 395 precipitation-induced runoff (rain-induced and snowmelt) during 1971–2020 in the YZ and its
 396 NX and NX-BXK basins are shown in Figure 10, and we also compare mean annual
 397 contribution of glacier runoff to total runoff between the drought years and all years for 1971–
 398 2020, suggesting that mean annual glacier contribution is greater in the drought years than all
 399 year. For example, glacier runoff contributes 29% to mean annual total runoff in the drought
 400 years in the NX-BXK, which is higher than its contribution (19%) for the period 1971–2020. It
 401 suggests that glacier runoff typically make a useful contribution to water supplies in study basin
 402 where summers are dry; however, glacier runoff shows limited roles in protecting water
 403 shortages from the drought in dry seasons in the YZ basin (Figure 10g–i), mostly due to the



404 limited glacier contribution compared to the water volume generated by rainfall in the
405 monsoon-dominated basins.

406

407 Glacier melt intensifies the flood frequency and severity among the basins in wet season (Figure
408 10 g–i). The flow duration curves (FDCs) for precipitation-induced runoff are lower than those
409 from total runoff, especially in the flood events (exceedance probability of > 95%), implying
410 increases in both the magnitude and frequency of maximum daily flow. In particular, in the time
411 series of runoff solely induced by precipitation (rainfall and snowmelt), peak flows higher than
412 2–8 mm/day typically have an exceedance frequency of 95%, while this exceedance frequency
413 is strongly reduced to 85%–90% in the time series of total runoff that is additionally fed by
414 glacier meltwater. In addition, the magnitudes of flood events in total runoff are higher in the
415 NX-BXK (exceedance probability of > 86%) than the NX basin (exceedance probability of >
416 90%), due to larger contribution of glacier runoff to total runoff in the NX-BXK sub-basin.

417

418 **5 Discussion**

419 **5.1 Runoff Changes in the Downstream Sub-basin**

420 The NX-BXK sub-basin, with the largest glacier area and runoff contribution to total runoff of
421 the YZ basin, is more sensitive to climate and cryosphere changes than the other sub-basins.
422 Therefore, runoff changes in this basin raise considerable concern for downstream life-
423 supporting water supplies.



424

425 Between existing research and our study, results are contradictory on runoff changes in the NX-
 426 BXK. Wang et al. (2021) suggested that total runoff showed an increasing trend of 6.4×10^8
 427 m^3/yr during 1998–2019. However, in our study, simulated total runoff exhibited a decreasing
 428 trend of about $-0.3 \text{ mm}/10\text{yr}$ ($-7.5 \times 10^8 \text{ m}^3/\text{yr}$) during 1998–2020 in the sub-basin (Figure 8,
 429 Table 3). This difference between the two studies is mostly because of the trends in precipitation
 430 estimates used for the hydrological model (Figure 11). Precipitation shows increasing trends of
 431 $90 \text{ mm}/10\text{yr}$ during 1981–2016 and $19 \text{ mm}/10\text{yr}$ during 1998–2016 in Wang et al. (2021),
 432 compared with decreasing trends of $-110.0 \text{ mm}/10\text{yr}$ during 1981–2016 and $-84.0 \text{ mm}/10\text{yr}$
 433 during 1998–2016 in this study. In addition, a decreasing trend of atmospheric moisture during
 434 the monsoon season in the sub-basin also partly confirms the rationality of the reconstructed
 435 precipitation used in this study as model input.

436

437 The variation of precipitation datasets for high mountains may result in large differences in
 438 meltwater contribution (Sun and Su, 2020). Less attention about the contribution of glacier
 439 runoff in the YZ basin was paid to the NX-BXK (Table 4), and large inconsistencies in glacier
 440 contributions also existed in these studies (Table 4), mostly resulting from uncertainties in
 441 forcing inputs and parameters for VIC-Glacier models. For example, Sun and Su (2020)
 442 suggested that mean annual glacier runoff contributed of about 45% to total runoff in the NX-
 443 BXK sub-basin for 1980–2000 using a hydrological model without calibration and validation



444 due to a lack of runoff observation in the sub-basin. Based on newly collected rain gauge data,
445 and runoff, glacier mass balance, and glacier and snow cover observations in the NX-BXK,
446 glacier runoff is simulated by the well-validated VIC-Glacier model forced by a
447 comprehensively reconstructed long-term precipitation dataset in this study. The contribution
448 of glacier runoff to total runoff is updated to 19% during 1971–2020 in the NX-BXK sub-basin.
449
450 Reliable parameters are crucial for accurate runoff simulation by hydrological models. The
451 DDF is the most sensitive parameter for degree-day glacier model (Hock, 2003). Zhang et al.
452 (2013) studied the sensitivity of glacier melt runoff to the parameters of DDFs, suggesting that
453 average annual glacier runoff would decrease/increase about 10% with the decrease/increase of
454 each one unit ($\text{mm } ^\circ\text{C}^{-1} \text{ day}^{-1}$) in DDF. In this work, the DDF parameters used in this study are
455 derived based on observed glacier mass balance data, but intensively validations on glacier melt
456 (e.g. observed glacier mass balance and satellite-based glacier area estimates). In addition,
457 monthly runoff observation from eight hydrological stations are collected to further validate
458 parameters, ensuring that the model set-up is suitable for our modelling purposes.

459

460 **5.2 Implications for Water Management**

461 Comprehensive understanding of regional runoff characteristics and changes shows important
462 implications for water management in the river basin. First, runoff regimes and changes are
463 different among the sub-basins of the YZ; thus, our findings of regional runoff changes among



464 sub-basins of the YZ basin are important to make informed policy decisions on local water
465 management. For instance, for the LS and NX basin, increased flows occur in April–September
466 related to increased rainfall and snowmelt peak to earlier spring, which may thus alleviate a
467 shortage of irrigation water in the drought-prone early stages of the growing season (Immerzeel
468 et al., 2010). On the contrary, for the NX-BXK basin, decreased flows are mostly occurred in
469 September–May related to decreased rainfall and snowmelt, which may be paid attention by
470 hydrological government to considerable effects on water security, stress, and availability. In
471 addition, climate changes have resulted in an increase of nature hazards largely associated with
472 cryosphere in recent years, such as glacier lake outburst floods and glacier collapses. On 16 and
473 29 October 2018, a glacier collapse blocked main course of the river and generated a dam-
474 breaching flood in the downstream sub-basin of the YZ, which threatened the living security of
475 more than 20,000 people in the Mainling County and Medog County (Chen et al., 2020; An et
476 al., 2021; Zhao et al., 2022). Therefore, effects of glacier change on hydrological processes
477 need to be further investigated, and early warning of nature hazards associated with cryosphere
478 is suggested to be placed emphasis in the NX-BXK, which accounts for about 65% of total
479 glacier area and about 52% of runoff in the YZ (Table 1).

480

481 Second, the YZ basin are threatened by hazard from both extreme floods and hydrological
482 drought (Figure 10). Therefore, our findings will be benefit to make informed policy decisions
483 on protecting downstream populations from the worst effects of the flood and drought events.



484 The Yarlung-Brahmaputra basin is one of the world's largest and most populated region,
485 providing life-supporting services to about 70 million people from the China, India, Bangladesh
486 and Bhutan countries (Pradhan et al., 2021). Higher flood risks in wet season and drought risks
487 in dry season will be particularly relevant for human safety and agricultural production in both
488 the upper and downstream basins of the YZ (Liu et al., 2018; Gao et al., 2019). Especially for
489 downstream region, vast agriculture areas along the main rivers and in the delta's floodplain
490 will likely experience higher flood water levels from upper regions, thus having higher risks of
491 reduced productivity and crop failure (Hoang et al., 2016). Therefore, some mitigation and
492 adaptation strategies are urgently needed to solve water security problems from flood or drought
493 hazard in this basin. Our study offers a basic framework for clarifying the extreme flood and
494 drought events, and investigating the roles of glacier runoff in extreme events in the monsoon-
495 dominated basin of the TP.

496

497 **6 Conclusions**

498 In this study, runoff regimes, flow changes and the attribution are comprehensively investigated
499 across six sub-basins in the YZ for 1971–2020 with a particular focus on the comparison
500 between the NX and NX-BXK based on a newly generated precipitation dataset and the well-
501 validated large-scale VIC-Glacier model with observed streamflow at eight hydrological
502 stations, glacier mass balance data at two sites, and satellite-based glacier and snow cover
503 estimates. Large regional differences in runoff regimes and flow changes in the YZ basin were



504 observed. The main features of these differences are summarized below.

505

506 1. Regional differences in runoff regimes are presented in the YZ basin. The NX-BXK
507 contributes 52% to total runoff at the Pasighat outlet of the YZ basin, followed by the YC-NX
508 (25%), LS (10%), and other sub-basins (3%–6%). Although runoff generation in the entire YZ
509 is dominated by rain-induced (59%–72%), glacier runoff plays more important roles in annual
510 total runoff in the downstream sub-basins (16%–19%) than other sub-basins, especially in
511 summer (23%–35%).

512

513 2. Regional differences in annual runoff changes are found in the YZ basin. Annual runoff
514 generally increases during 1971–2020 in all sub-basins of the NX basin (8–19 mm/10yr), except
515 for the RKZ sub-basin. The NX-BXK sub-basin (–9.4 mm/10yr, $p < 0.05$) shows a significant
516 decrease, which results in a weak increasing trend of 3.1 mm/10yr in the entire YZ basin. Total
517 runoff trends reverse after 1998 for all the sub-basins of the YZ, with increasing trends during
518 1971–1997 and decreasing trends during 1998–2020. However, the decreasing trend of total
519 runoff is slower in the NX-BXK (–0.3 mm/10yr) than the NX (–3.3 mm/10yr) due to the stronger
520 increases of glacier runoff (16.1 mm/10yr) in the NX-BXK. Annual runoff changes in the YZ
521 and its six sub-basins are dominated by precipitation-induced runoff from non-glacierized areas,
522 with only minor impacts from glacier runoff.

523



524 3. Regional differences in seasonal runoff changes are apparent in the YZ basin. Relative to
525 1971–1997, mean monthly total runoff increased by 5%–22% in NX for 1998–2020, mostly
526 due to increases in rain-induced and glacier runoff, while monthly runoff decreased by 3%–20%
527 in NX-BXK because of decreases in precipitation-induced runoff. As an integrated result of
528 seasonal runoff changes in these basins, total runoff in the YZ basin increased by 3%–20%
529 during June–September, primarily due to increases in rain-induced and glacier runoff, while
530 total runoff decreased in the other months because of decreased precipitation-induced runoff.

531

532 4. Regional differences in extreme frequency of flood and drought are apparent in the YZ basin.
533 The NX basin faces a considerably hazard from extreme flood, with an increasing trend of 6
534 days/10yr. However, more severe hydrological droughts are likely to exacerbate ongoing water
535 stress in the NX-BXK sub-basin.

536

537 5. Regional differences in the importance of glacier runoff to water supplies are apparent in the
538 YZ basin. Glacier runoff plays an increasing role in both annual and seasonal water supplies
539 during 1971–2020 in the entire YZ as well as in its NX-BXK sub-basin. This is evidenced by
540 increased glacier runoff and its contribution to total runoff. Glacier runoff shows limited roles
541 in mitigating water shortages caused by the drought in dry seasons in the YZ basin, but it
542 intensifies flood frequency and severity among the basins in wet season.

543



544 **Acknowledgments**

545 This study was financially supported by the National Natural Science Foundation of China
546 (42201140), project funded by China Postdoctoral Science Foundation (2022M723256), and
547 the Second Tibetan Plateau Scientific Expedition and Research (STEP) Program
548 (2019QZKK0201). We also thank Daqing Yang and Ying Li for their constructive suggestions.

549

550 **Code and data availability**

551 The first Chinese Spatial Glacier Inventory is available from <http://westdc.westgis.ac.cn/glacier>.
552 The Randolph Glacier Inventory 6.0 is available from <http://www.glims.org/RGI/>. The snow
553 cover area data of the MODIS 10CM are available from <https://nsidc.org/data>. Observed runoff
554 data are from the Tibetan Hydrological Bureaus. Observed glacier mass balance data at
555 Gurenhekou and Parlung No.94 are collected from the Institute of Tibetan Plateau Research,
556 Chinese Academy of Sciences (<http://www.tpsc.ac.cn>). All codes used to produce the results
557 are available upon request to the authors.

558

559 **Author Contributions**

560 He Sun: Conceptualization, Formal analysis, Investigation, Methodology, Resources,
561 Visualization, Funding acquisition, Writing draft. Tandong Yao: Conceptualization, Resources,
562 Visualization, Funding acquisition, Writing (review and editing). Fengge Su: Writing (review
563 and editing). Wei Yang: Editing and providing glacier mass balance data. Guifeng Huang:



564 Methodology, Resources. Deliang Chen: Writing (review and editing).

565

566 **Competing interests**

567 The authors declare that they have no known competing financial interests or personal
 568 relationships that could have appeared to influence the work reported in this paper.

569

570 **References**

- 571 An, B., Wang, W., Yang, W., Wu, G., Guo, Y., Zhu, H., Gao, Y., Bai, L., Zhang, F., Zeng, C.,
 572 Wang, L., Zhou, J., Li, X., Li, J., Zhao, Z., Chen, Y., Liu, J., Li, J., Wang, Z., Chen, W., and Yao,
 573 T.: Process, mechanisms, and early warning of glacier collapse-induced river blocking disasters
 574 in the Yarlung Tsangpo Grand Canyon, southeastern Tibetan Plateau, Sci Total Environ, 151652,
 575 <https://doi.org/10.1016/j.scitotenv.2021.151652>, 2021.
- 576 Bahr, D. B., Meier, M. F., and Peckham, S. D.: The physical basis of glacier volume - area
 577 scaling, J. Geophys. Res. Solid Earth, 102, 20355-20362, <https://doi.org/10.1029/97jb01696>,
 578 1997.
- 579 Barnett, T. P., Adam, J. C., and Lettenmaier, D. P.: Potential impacts of a warming climate on
 580 water availability in snow-dominated regions, Nature, 438, 303-309,
 581 <https://doi.org/10.1038/nature04141>, 2005.
- 582 Chen, C., Zhang, L., Xiao, T., and He, J.: Barrier lake bursting and flood routing in the Yarlung
 583 Tsangpo Grand Canyon in October 2018, J. Hydrol., 583,
 584 <https://doi.org/10.1016/j.jhydrol.2020.124603>, 2020.



- 585 Chen, X., Long, D., Hong, Y., Zeng, C., and Yan, D.: Improved modeling of snow and glacier
 586 melting by a progressive two-stage calibration strategy with GRACE and multisource data:
 587 How snow and glacier meltwater contributes to the runoff of the Upper Brahmaputra River
 588 basin?, *Water Resour. Res.*, 53, 2431–2466, <https://doi.org/10.1002/2016WR019656>, 2017.
- 589 Cuo, L. and Zhang, Y.: Spatial patterns of wet season precipitation vertical gradients on the
 590 Tibetan Plateau and the surroundings, *Sci. Rep.*, 7, 5057, [https://doi.org/10.1038/s41598-017-](https://doi.org/10.1038/s41598-017-05345-6)
 591 05345-6, 2017.
- 592 Cuo, L., Li, N., Liu, Z., Ding, J., Liang, L., Zhang, Y., and Gong, T.: Warming and human
 593 activities induced changes in the Yarlung Tsangpo basin of the Tibetan plateau and their
 594 influences on streamflow, *J. Hydrol-Reg. Stud.*, 25, <https://doi.org/10.1016/j.ejrh.2019.100625>,
 595 2019.
- 596 Duethmann, D., Peters, J., Blume, T., Vorogushyn, S., and Güntner, A.: The value of satellite-
 597 derived snow cover images for calibrating a hydrological model in snow-dominated catchments
 598 in Central Asia, *Water Resour. Res.*, 50, 2002–2021, <https://doi.org/10.1002/2013wr014382>,
 599 2014.
- 600 Gao, C., Liu, L., Ma, D., He, K., and Xu, Y. P.: Assessing responses of hydrological processes
 601 to climate change over the southeastern Tibetan Plateau based on resampling of future climate
 602 scenarios, *Sci Total Environ*, 664, 737–752, <https://doi.org/10.1016/j.scitotenv.2019.02.013>,
 603 2019.
- 604 Hoang, L. P., Lauri, H., Kummu, M., Koponen, J., van Vliet, M. T. H., Supit, I., Leemans, R.,



- 605 Kabat, P., and Ludwig, F.: Mekong River flow and hydrological extremes under climate change,
 606 Hydrol. Earth Syst. Sci., 20, 3027-3041, 10.5194/hess-20-3027-2016, 2016.
- 607 Hock, R.: Temperature index melt modelling in mountain areas, J. Hydrol., 282, 104-115,
 608 [https://doi.org/10.1016/s0022-1694\(03\)00257-9](https://doi.org/10.1016/s0022-1694(03)00257-9), 2003.
- 609 Kan, B., Su, F., Xu, B., Xie, Y., Li, J., and Zhang, H.: Generation of High Mountain Precipitation
 610 and Temperature Data for a Quantitative Assessment of Flow Regime in the Upper Yarkant
 611 Basin in the Karakoram, J. Geophys. Res. Atmos., 123, 8462-8486,
 612 <https://doi.org/10.1029/2017jd028055>, 2018.
- 613 Li, C., Su, F., Yang, D., Tong, K., Meng, F., and Kan, B.: Spatiotemporal variation of snow
 614 cover over the Tibetan Plateau based on MODIS snow product, 2001-2014, Int. J. Climatol.,
 615 38, 708-728, <https://doi.org/10.1002/joc.5204>, 2018.
- 616 Liang, X., Lettenmaier, D. P., and Wood, E. F.: One-dimensional statistical dynamic
 617 representation of subgrid spatial variability of precipitation in the two-layer variable infiltration
 618 capacity model, J. Geophys. Res. Atmos., 101, 21403-21422,
 619 <https://doi.org/10.1029/96jd01448>, 1996.
- 620 Liang, X., Lettenmaier, D. P., Wood, E. F., and Burges, S. J.: A simple hydrologically based
 621 model of land-surface water and energy fluxes, J. Geophysical Research, 99:, 14415–14428,
 622 <https://doi.org/10.1029/94jd00483>, 1994.
- 623 Liu, L., Pan, S. L., Bai, Z. X., and Xu, Y. P.: Potential application of hydrological ensemble
 624 prediction in forecasting flood and its components over the Yarlung Zangbo River Basin, China,



- 625 Hydrol. Earth Syst. Sci. Discuss., 1-33, <https://doi.org/10.5194/hess-2018-179>, 2018.
- 626 Liu, L., Gu, H., Xie, J., and Xu, Y. P.: How well do the ERA - Interim, ERA - 5, GLDAS - 2.1
 627 and NCEP - R2 reanalysis datasets represent daily air temperature over the Tibetan Plateau?,
 628 Int. J. Climatol., <https://doi.org/10.1002/joc.6867>, 2020.
- 629 Liu, S., Sun, W., Shen, Y., and Li, G.: Glacier changes since the Little Ice Age maximum in the
 630 western Qilian Shan, northwest China, and consequences of glacier runoff for water supply, J.
 631 Glaciol., 49, 117-124, <https://doi.org/10.3189/172756503781830926>, 2003.
- 632 Liu, Y., Wu, G., Hong, J., Dong, B., Duan, A., Bao, Q., and Zhou, L.: Revisiting Asian monsoon
 633 formation and change associated with Tibetan Plateau forcing: II. Change, Clim. Dynam., 39,
 634 1183-1195, <https://doi.org/10.1007/s00382-012-1335-y>, 2012.
- 635 Lutz, A. F., Immerzeel, W. W., Kraaijenbrink, P. D., Shrestha, A. B., and Bierkens, M. F.:
 636 Climate Change Impacts on the Upper Indus Hydrology: Sources, Shifts and Extremes, PLoS
 637 One, 11, e0165630, <https://doi.org/10.1371/journal.pone.0165630>, 2016.
- 638 Meng, F. C., Su, F. G., Li, Y., and Tong, K.: Changes in Terrestrial Water Storage During 2003-
 639 2014 and Possible Causes in Tibetan Plateau, J. Geophys. Res. Atmos., 124, 2909-2931,
 640 <https://doi.org/10.1029/2018jd029552>, 2019.
- 641 Miao, L., Li, S., Zhang, F., Chen, T., Shan, Y., and Zhang, Y.: Future Drought in the Dry Lands
 642 of Asia Under the 1.5 and 2.0 °C Warming Scenarios, Earth's Future, 8,
 643 <https://doi.org/10.1029/2019ef001337>, 2020.
- 644 Niu, Q., Liu, L., Heng, J., Li, H., and Xu, Z.: A Multi-Index Evaluation of Drought



- 645 Characteristics in the Yarlung Zangbo River Basin of Tibetan Plateau, Southwest China, *Front.*
 646 *Earth Sc.*, 8, <https://doi.org/10.3389/feart.2020.00213>, 2020.
- 647 Pradhan, N. S., Das, P. J., Gupta, N., and Shrestha, A. B.: Sustainable Management Options for
 648 Healthy Rivers in South Asia: The Case of Brahmaputra, *Sustainability*, 13,
 649 <https://doi.org/10.3390/su13031087>, 2021.
- 650 Pritchard, H. D.: Asia's shrinking glaciers protect large populations from drought stress, *Nature*,
 651 569, 649-654, <https://doi.org/10.1038/s41586-019-1240-1>, 2019.
- 652 Su, F., Hong, Y., and Lettenmaier, D. P.: Evaluation of TRMM Multisatellite Precipitation
 653 Analysis (TMPA) and Its Utility in Hydrologic Prediction in the La Plata Basin, *J.*
 654 *Hydrometeorol.*, 9, 622-640, <https://doi.org/10.1175/2007jhm944.1>, 2008.
- 655 Su, F., Zhang, L., Ou, T., Chen, D., Yao, T., Tong, K., and Qi, Y.: Hydrological response to
 656 future climate changes for the major upstream river basins in the Tibetan Plateau, *Glob. Planet.*
 657 *Change*, 136, 82-95, <https://doi.org/10.1016/j.gloplacha.2015.10.012>, 2016.
- 658 Su, F., Pritchard, H. D., Yao, T., Huang, J., Ou, T., Meng, F., Sun, H., Li, Y., Xu, B., Zhu, M.,
 659 and Chen, D.: Contrasting Fate of Western Third Pole's Water Resources Under 21st Century
 660 *Climate Change, Earth's Future*, 10, <https://doi.org/10.1029/2022ef002776>, 2022.
- 661 Sun, H. and Su, F.: Precipitation correction and reconstruction for streamflow simulation based
 662 on 262 rain gauges in the upper Brahmaputra of southern Tibetan Plateau, *J. Hydrol.*, 590,
 663 <https://doi.org/10.1016/j.jhydrol.2020.125484>, 2020.
- 664 Sun, H., Su, F., He, Z., Ou, T., Chen, D., Li, Z., and Li, Y.: Hydrological evaluation of high-



665 resolution precipitation estimates from the WRF model in the Third Pole river basins, J.
 666 Hydrometeorol., <https://doi.org/10.1175/jhm-d-20-0272.1>, 2021.

667 Sun, H., Yao, T., Su, F., He, Z., Tang, G., Li, N., Zheng, B., Huang, J., Meng, F., and Ou, T. J.
 668 J. o. H.: Corrected ERA5 precipitation by machine learning significantly improved flow
 669 simulations for the Third Pole basins, J. Hydrometeorol., 23, [https://doi.org/10.1175/JHM-D-](https://doi.org/10.1175/JHM-D-22-0015.1)
 670 22-0015.1, 2022.

671 Tong, K., Su, F., and Xu, B.: Quantifying the contribution of glacier meltwater in the expansion
 672 of the largest lake in Tibet, J. Geophys. Res. Atmos., 121, 11158-11173,
 673 <https://doi.org/10.1002/2016jd025424>, 2016.

674 Wang, A., Wang, Y., Su, B., Kundzewicz, Z. W., Tao, H., Wen, S., Qin, J., Gong, Y., and Jiang,
 675 T.: Comparison of Changing Population Exposure to Droughts in River Basins of the Tarim and
 676 the Indus, Earth's Future, 8, <https://doi.org/10.1029/2019ef001448>, 2020.

677 Wang, Y., Wang, L., Zhou, J., Yao, T., Yang, W., Zhong, X., Liu, R., Hu, Z., Luo, L., Ye, Q.,
 678 Chen, N., and Ding, H.: Vanishing glaciers at southeast Tibetan Plateau have not offset the
 679 declining runoff at Yarlung Zangbo, Geophys. Res. Lett., <https://doi.org/10.1029/2021gl094651>,
 680 2021.

681 Wu, G. and Duan, A.: Weakening Trend in the Atmospheric Heat Source over the Tibetan
 682 Plateau during Recent Decades. Part I: Observations, J. Clim., 21, 3149-3164,
 683 <https://doi.org/10.1175/2007jcli1912.1>, 2008.

684 Wu, G. and Duan, A.: Weakening Trend in the Atmospheric Heat Source over the Tibetan



- 685 Plateau during Recent Decades. Part II: Connection with Climate Warming, *J. Clim.*, 22, 4197-
 686 4212, <https://doi.org/10.1175/2009jcli2699.1>, 2009.
- 687 Yang, W., Yao, T., Guo, X., Zhu, M., Li, S., and Kattel, D. B.: Mass balance of a maritime
 688 glacier on the southeast Tibetan Plateau and its climatic sensitivity, *J. Geophys. Res. Atmos.*,
 689 118, 9579-9594, <https://doi.org/10.1002/jgrd.50760>, 2013.
- 690 Yang, W., Guo, X., Yao, T., Yang, K., Zhao, L., Li, S., and Zhu, M.: Summertime surface energy
 691 budget and ablation modeling in the ablation zone of a maritime Tibetan glacier, *J. Geophys.*
 692 *Res. Atmos.*, 116, <https://doi.org/10.1029/2010jd015183>, 2011.
- 693 Yang, Y., Gao, D., and Li, B.: Study on the moisture passage on the lower reaches of the Yarlung
 694 Zangbo river, *Sci. China (Series B)* 32, 580-593, 1989.
- 695 Yang, Z., Zhuo, M., Lu, H., Ma, P., and Zhou, K.: Characteristics of precipitation variation and
 696 its effects on runoff in the Yarlung Zangbo River basin during 1961–2010, *Journal of*
 697 *Glaciology and Geocryology*, 36, 166-172 (in chinese), 2014b.
- 698 Yao, T.: Recent glacial retreat in High Asia in China and its impact on water resource in
 699 Northwest China, *Sci. China (Series D)*, 47, 1065, <https://doi.org/10.1360/03yd0256>, 2004.
- 700 Yao, T., Thompson, L., Yang, W., Yu, W., Gao, Y., Guo, X., Yang, X., Duan, K., Zhao, H., Xu,
 701 B., Pu, J., Lu, A., Xiang, Y., Kattel, D. B., and Joswiak, D.: Different glacier status with
 702 atmospheric circulations in Tibetan Plateau and surroundings, *Nat. Clim. Chang.*, 2, 663-667,
 703 <https://doi.org/10.1038/nclimate1580>, 2012.
- 704 Zhang, L., Su, F., Yang, D., Hao, Z., and Tong, K.: Discharge regime and simulation for the



705 upstream of major rivers over Tibetan Plateau, *J. Geophys. Res. Atmos.*, 118, 8500-8518,
 706 <https://doi.org/10.1002/jgrd.50665>, 2013.

707 Zhao, C., Yang, W., Westoby, M., An, B., Wu, G., Wang, W., Wang, Z., Wang, Y., and Dunning,
 708 S.: Brief communication: An approximately 50 Mm³ ice-rock
 709 avalanche on 22 March 2021 in the Sedongpu valley, southeastern Tibetan Plateau, *The*
 710 *Cryosphere*, 16, 1333-1340, <https://doi.org/10.5194/tc-16-1333-2022>, 2022.

711 Zhao, Q., Ding, Y., Wang, J., Gao, H., Zhang, S., Zhao, C., Xu, J., Han, H., and Shangguan, D.:
 712 Projecting climate change impacts on hydrological processes on the Tibetan Plateau with model
 713 calibration against the Glacier Inventory Data and observed streamflow, *J. Hydrol.*, 573, 60-81,
 714 <https://doi.org/10.1016/j.jhydrol.2019.03.043>, 2019.

715 Zhong, L., Ma, Y., Fu, Y., Pan, X., Hu, W., Su, Z., Salama, M. S., and Feng, L.: Assessment of
 716 soil water deficit for the middle reaches of Yarlung-Zangbo River from optical and passive
 717 microwave images, *Remote Sens. Environ.*, 142, 1-8, <https://doi.org/10.1016/j.rse.2013.11.008>,
 718 2014.



Captions:

Figure 1. Location and topography of the Yarlung Zangbo (YZ) river basin. Numbers 1 to 6 show the sub-basins of Lhatse (LZ), Lhatse-Yangcun (LZ-YC), Shigatse (RKZ), Lhasa (LS), Yangcun-Nuxia (YC-NX), and Nuxia-Pasighat (NX-BXK), respectively.

Figure 2. Annual time series of observed and simulated glacier mass balance at (a) Gurenhekou for 2005–2009 and (b) Parlung No.94 for 2006–2018, and (c) mean annual glacier coverage (%) during 2000–2010 from the VIC-Glacier model simulation and satellite-based observation over the entire YZ basin and its sub-basins.

Figure 3. (a) Time series and (b) flow duration curve of observed and simulated daily runoff at Nuxia hydrological station for 1971–1980.

Figure 4. Mean monthly observed and simulated runoff at eight hydrological stations of sub-basins in the YZ for 1971–2015 (1981–2000 for YG and 2004–2013 for BM). Abbreviations LZ, RKZ, LS, LZ-YC, YC-NX, NX, YG and BM represent the upstream basins of Lhatse, Shigatse, Lhasa, the regions between Lhatse and Yangcun, between Yangcun and Nuxia, Nuxia, Yigong and Bomi, respectively.

Figure 5. Annual time series of observed and simulated runoff at nine hydrological stations in sub-basins of the YZ for 1971–2015 (1981–2000 for YG, 2004–2013 for BM and 2015–2019 for MT). Abbreviations LZ, RKZ, LS, LZ-YC, YC-NX, NX, YG, BM and MT represent the upstream basins of Lhatse, Shigatse, Lhasa, the regions between Lhatse and Yangcun, between Yangcun and Nuxia, Nuxia, Yigong, Bomi and Motuo, respectively. The asterisk indicates 95% significance confidence level.

Figure 6. Monthly time series of snow cover fraction (%) from the VIC-Glacier model simulation and satellite-based observations over the entire YZ basin and its four sub-basins for 2001–2019. The asterisk indicates 95% significance confidence level.

Figure 7. Mean monthly simulated rainfall, snowmelt, and glacier runoff, and their contribution to total annual runoff in the YZ and its sub-basins for 1971–2020.



Figure 8. Annual variations of precipitation, temperature, total runoff and three runoff components (rainfall, glacier and snowmelt runoff) in the YZ and its sub-basins for 1971–2020, respectively. Linear trends are indicated by dashed lines, and corresponding values are also indicated. Asterisks indicate the 95% significance level

Figure 9. Changes in (a–c) mean monthly total runoff, (d–f) three components, and (g–i) their contributions to total runoff for the period 1998–2020 relative to the period 1971–1997 in the entire YZ basin and its NX and NX-BXK sub-basins.

Figure 10. (a–c) Extreme flood and drought days, (d–f) annual maximum daily runoff, and (g–i) flow duration curves for simulated daily runoff during 1971–2020 in the YZ and its NX and NX-BXK basins.

Figure 11. Time series of annual precipitation estimates from different datasets in the NX-BXK sub-basin. Asterisks indicate the 95% significance level.

Table 1. Characteristics of the six sub-basins in the Yarlung Zangbo River.

Table 2. List of data used in this study for the VIC-Glacier model validation.

Table 3. Trends in precipitation, temperature, total runoff, and three runoff components and their contributions to total runoff in the YZ basins for different periods. Asterisks indicate the 95% confidence level.

Table 4. Summary of relevant studies on simulated runoff component contributions in the YZ basin.

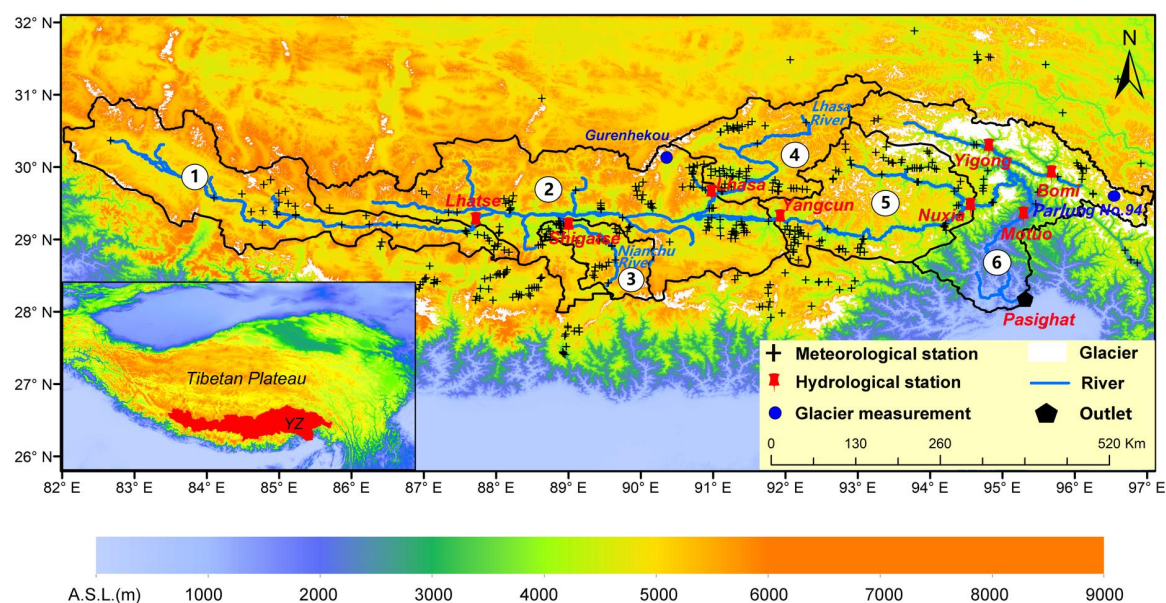


Figure 1. Location and topography of the Yarlung Zangbo (YZ) river basin. Numbers 1 to 6 show the sub-basins of Lhatse (LZ), Lhatse-Yangcun (LZ-YC), Shigatse (RKZ), Lhasa (LS), Yangcun-Nuxia (YC-NX), and Nuxia-Pasighat (NX-BXK), respectively.

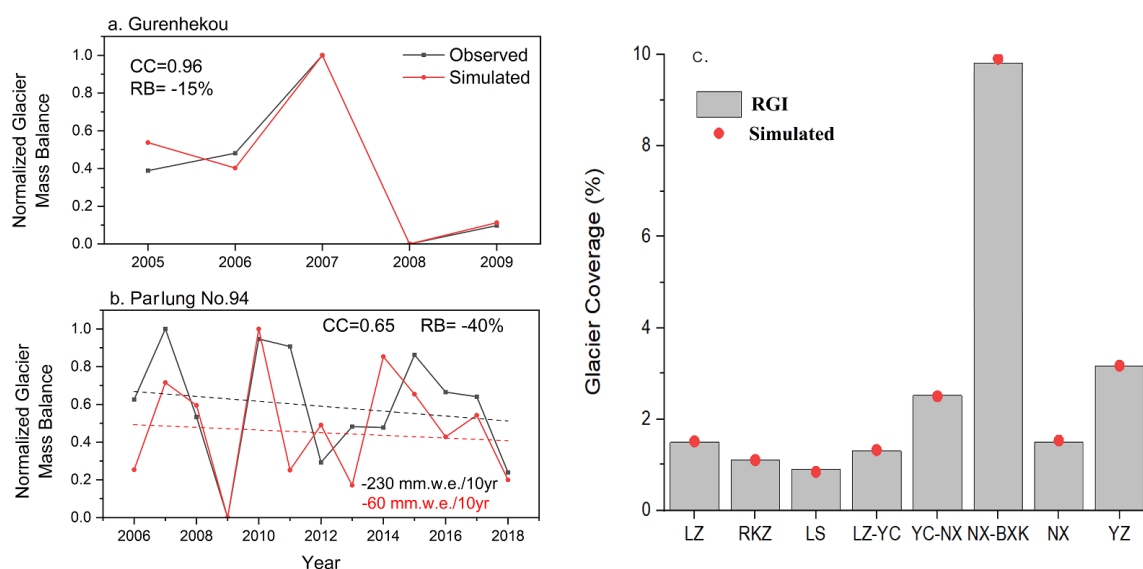


Figure 2. Annual time series of observed and simulated glacier mass balance at (a) Gurenhekou for 2005–2009 and (b) Parlung No.94 for 2006–2018, and (c) mean annual glacier coverage (%) during 2000–2010 from the VIC-Glacier model simulation and satellite-based observations over the entire YZ basin and its sub-basins. The number of each figure are calculated with actual magnitudes.

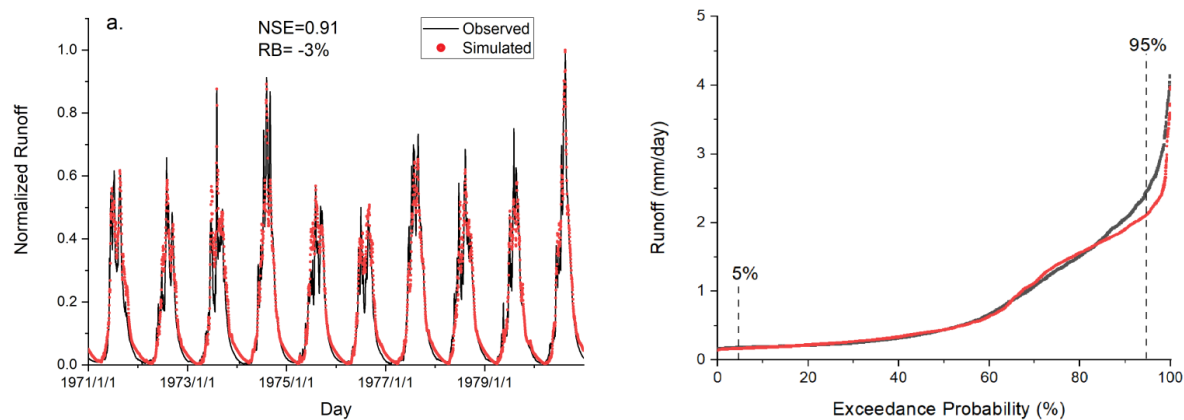


Figure 3. (a) Time series and (b) flow duration curve of observed and simulated daily runoff at Nuxia hydrological station for 1971–1980.

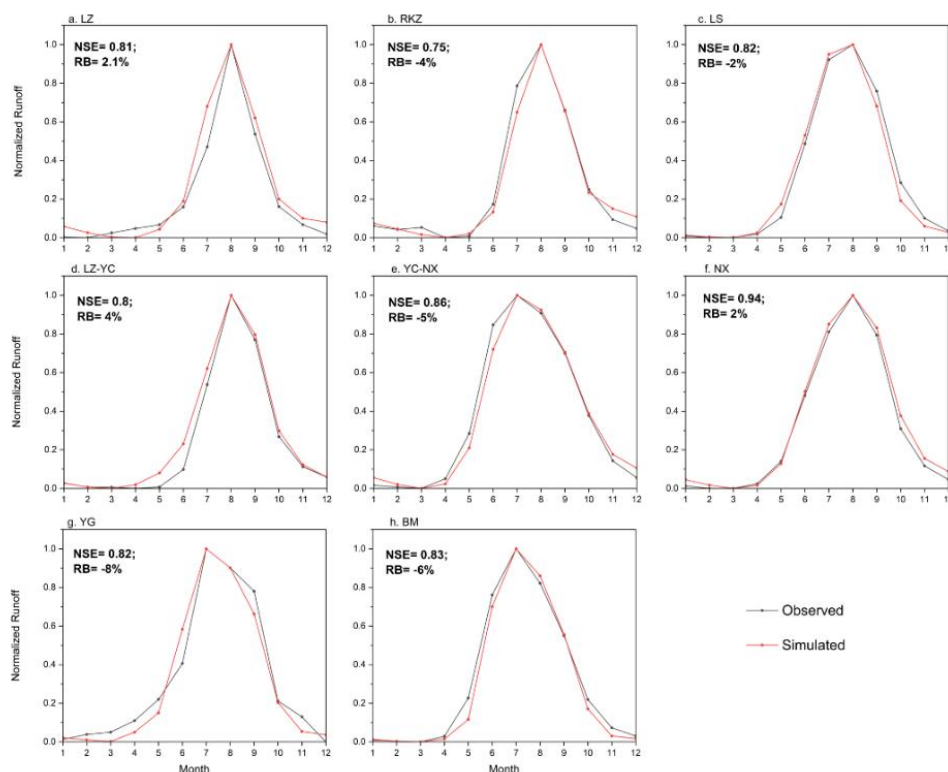


Figure 4. Mean monthly observed and simulated runoff at eight hydrological stations of sub-basins in the YZ for 1971–2015 (1981–2000 for YG and 2004–2013 for BM). Abbreviations LZ, RKZ, LS, LZ-YC, YC-NX, NX, YG and BM represent the upstream basins of Lhatse, Shigatse, Lhasa, the regions between Lhatse and Yangcun, between Yangcun and Nuxia, Nuxia, Yigong and Bomi, respectively. The number of each figure are calculated with actual magnitudes.

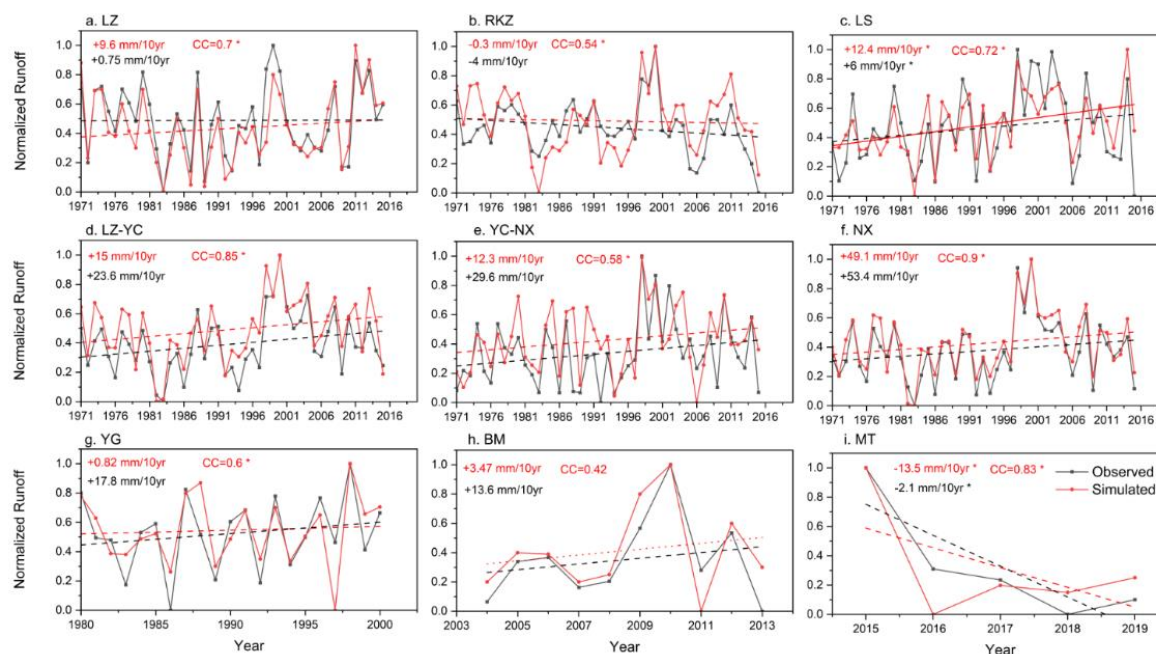


Figure 5. Annual time series of observed and simulated runoff at nine hydrological stations in sub-basins of the YZ for 1971–2015 (1981–2000 for YG, 2004–2013 for BM and 2015–2019 for MT). Abbreviations LZ, RKZ, LS, LZ-YC, YC-NX, NX, YG, BM and MT represent the upstream basins of Lhatse, Shigatse, Lhasa, the regions between Lhatse and Yangcun, between Yangcun and Nuxia, Nuxia, Yigong, Bomi and Motuo, respectively. The asterisk indicates 95% significance confidence level. The number of each figure are calculated with actual magnitudes.

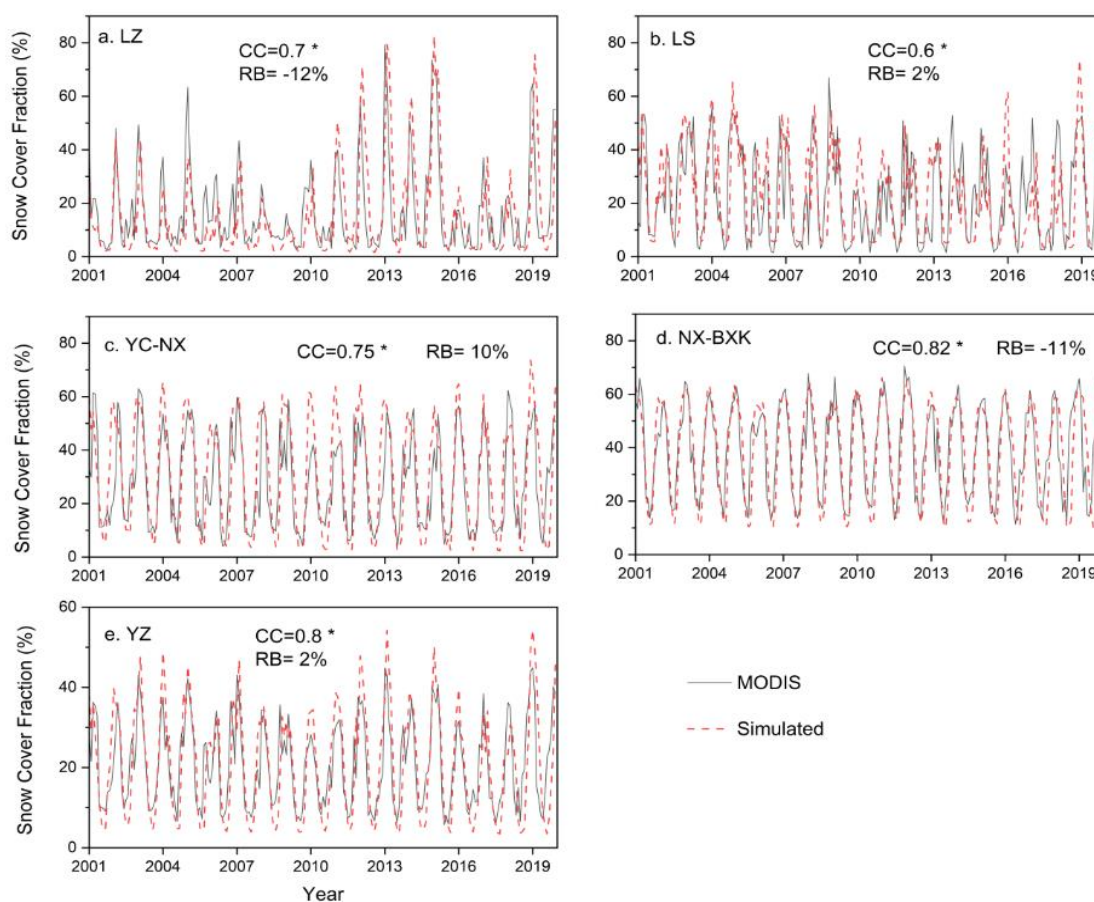


Figure 6. Monthly time series of snow cover fraction (%) from the VIC-Glacier model simulation and satellite-based observations over the entire YZ basin and its four sub-basins for 2001–2019. The asterisk indicates 95% significance confidence level.

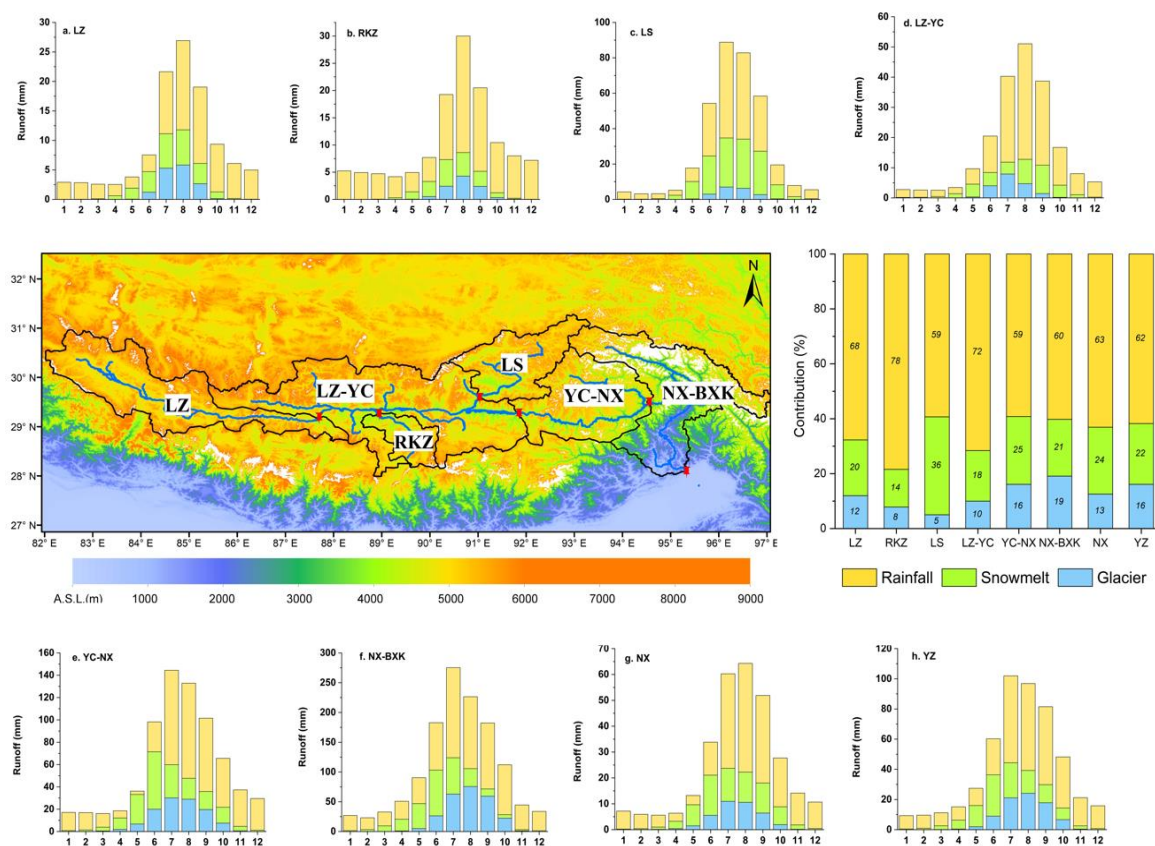


Figure 7. Mean monthly simulated rainfall, snowmelt, and glacier runoff, and their contribution to total annual runoff in the YZ and its sub-basins for 1971–2020.

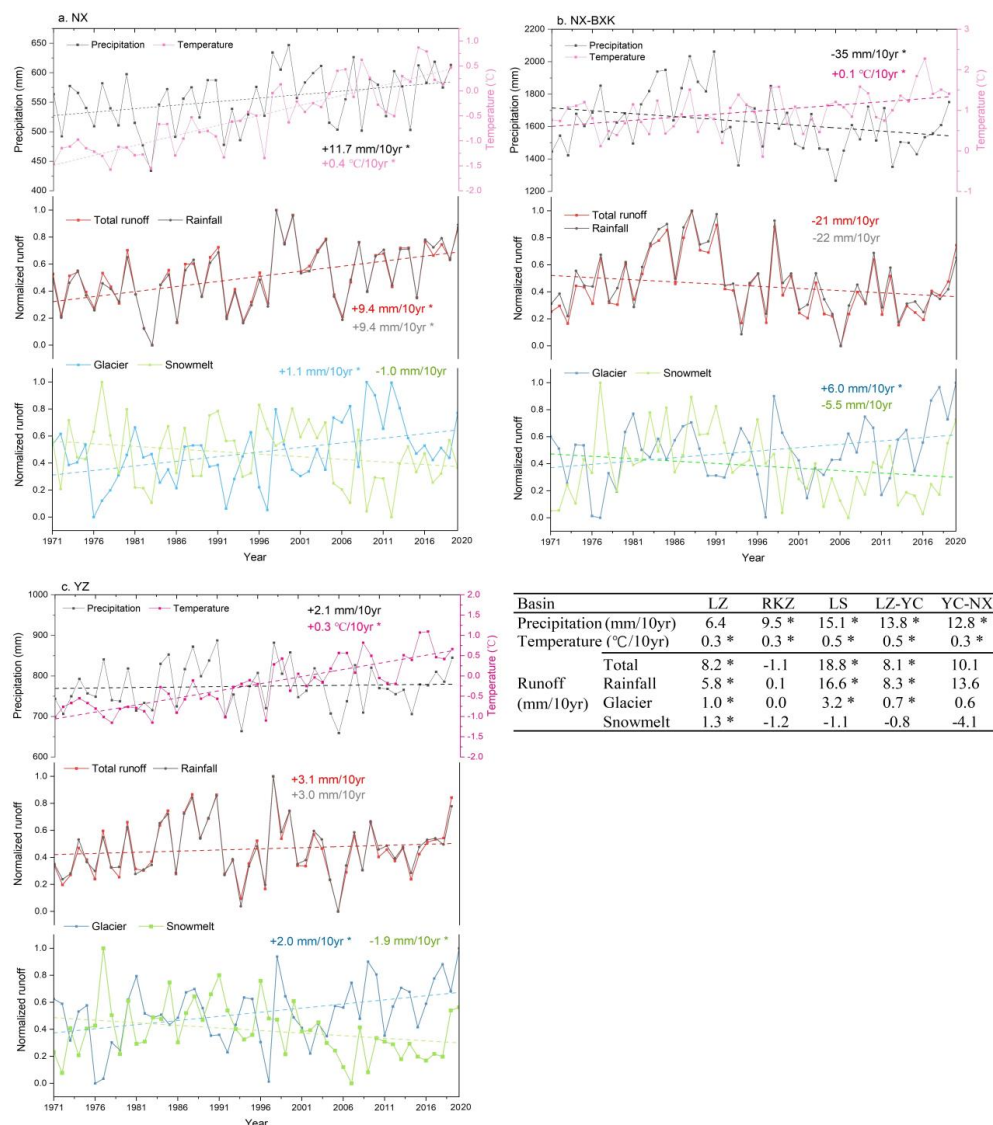


Figure 8. Annual variations of precipitation, temperature, total runoff, and three runoff components (rainfall, glacier, and snowmelt runoff) in the YZ and its sub-basins for 1971–2020, respectively. Linear trends are indicated by dashed lines, and corresponding values are also indicated. Tendency results for sub-basins are shown in the inset table. The number of each figure are calculated with actual magnitudes. Asterisks indicate the 95% significance level.

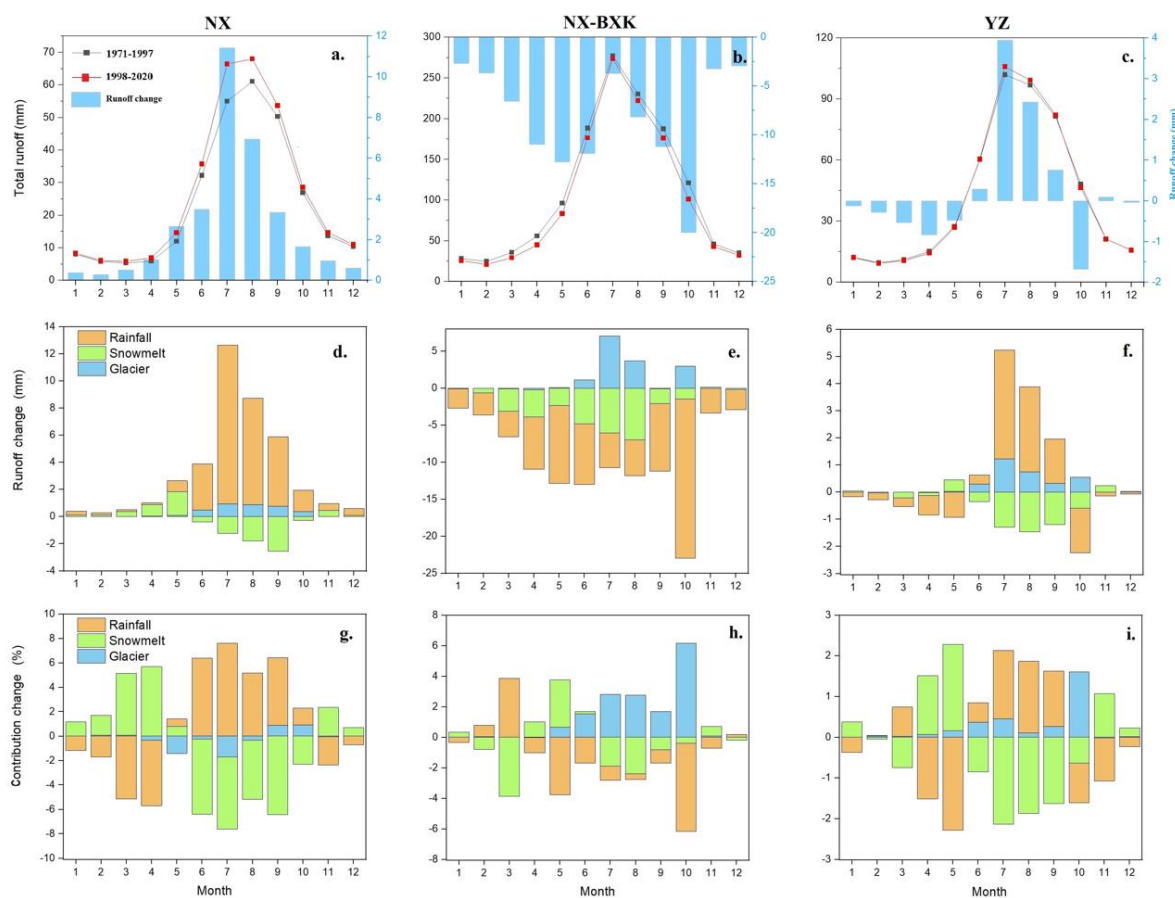


Figure 9. Changes in (a–c) mean monthly total runoff, (d–f) three components, and (g–i) their contributions to total runoff for the period 1998–2020 relative to the period 1971–1997 in the entire YZ basin and its NX and NX-BXK sub-basins.

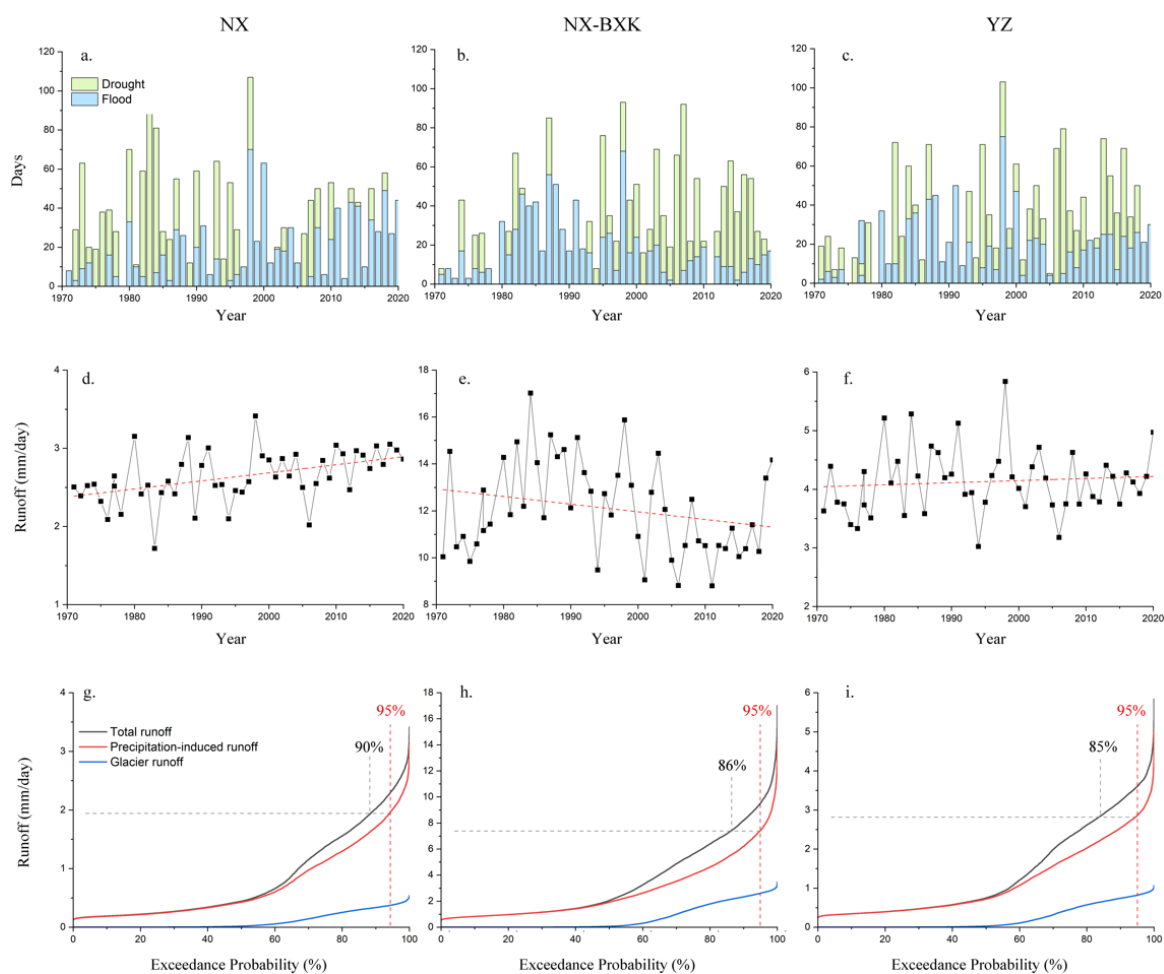


Figure 10. (a–c) Extreme flood and drought days, (d–f) annual maximum daily runoff, and (g–i) flow duration curves for simulated daily runoff during 1971–2020 in the YZ and its NX and NX-BXK basins.

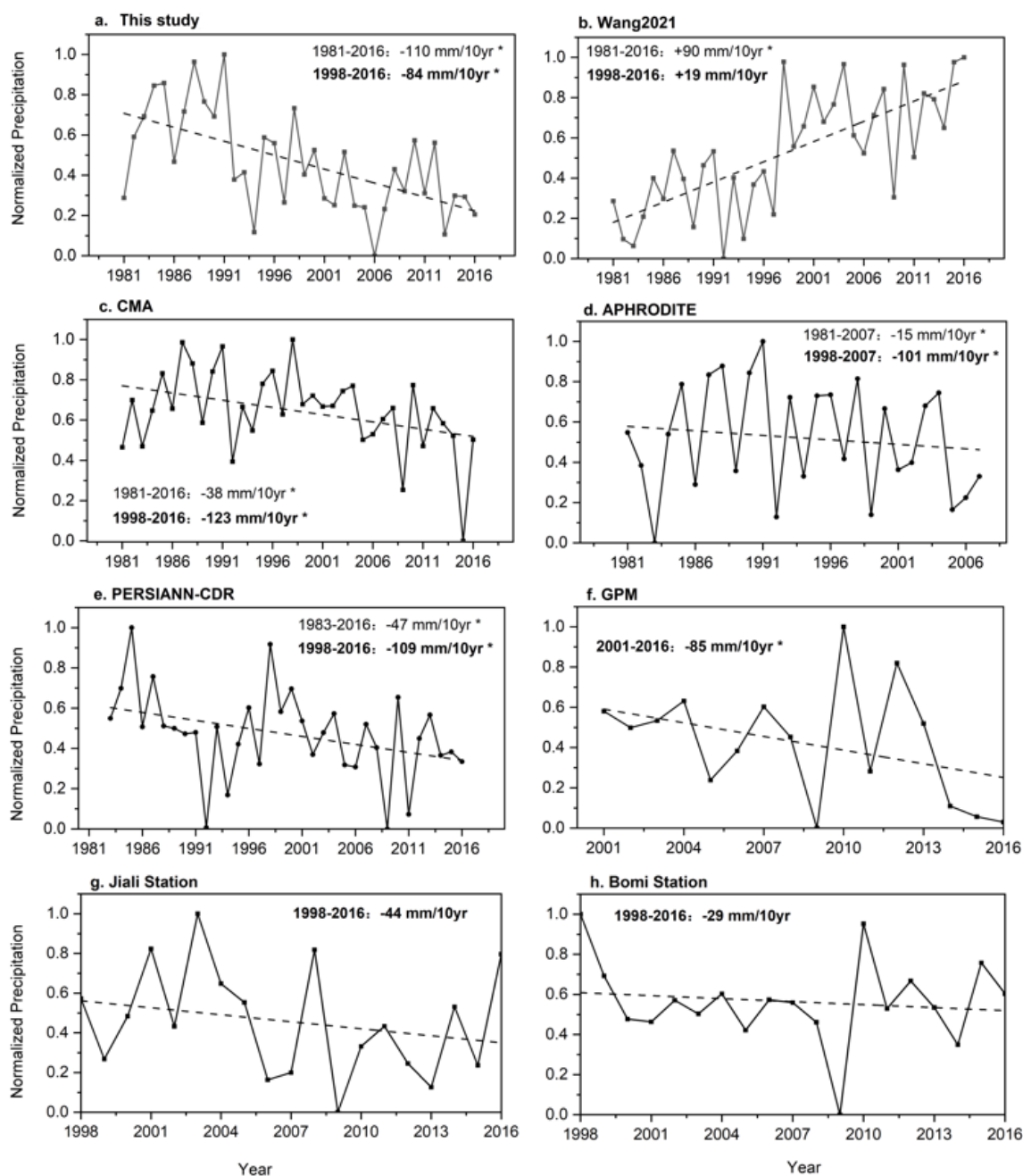


Figure 11. Time series of annual precipitation estimates from different datasets in the NX-BXK sub-basin.

Asterisks indicate the 95% significance level.



Table 1. Characteristics of the six sub-basins in the Yarlung Zangbo River

		LZ	LZ-YC	RKZ	LS	YC-NX	NX-BXK	YZ
Outlet		Lhatse	Yangcun	Shigatse	Lhasa	Nuxia	Pasighat	Pasighat
Hydrological station	Name	Lhatse	Yangcun	Shigatse	Lhasa	Nuxia	Motuo	—
	Latitude (°N)	29.05	29.28	29.25	29.63	29.47	29.32	—
	Longitude (°E)	87.38	91.88	88.88	91.15	94.57	95.29	—
Drainage area (km ²)		50553	71926	11064	26235	41770	51507	253,055
Basin average elevation (m)		5370	4767	5353	5272	4937	3711	4901
Mean annual precipitation (mm) *		283	417	361	564	939	1465	774
Mean annual temperature (°C) *		-2.91	0.24	1.73	-1.28	0.97	1.21	-0.2
Glacier area (km ²)		809	640	134	257	1174	5259	8273
Glacier coverage (%) **		1.60	0.89	1.21	0.98	2.81	10.21	3.27
Degree day factor (mm °C ⁻¹ day ⁻¹)		10.97	10.97	10.97	9.2	6.8	6.5	—
Snow cover area (km ²)		7876	7344	772	6055	10129	16467	48643
Snow cover fraction (%)		15.58	10.21	6.98	23.08	24.25	31.97	19.22

*The periods of precipitation and temperature data are from 1961 to 2020.

**Glacier data are from the first China Glacier Inventory, <http://westdc.westgis.ac.cn/glacier>.



Table 2. List of data used in this study for the VIC-Glacier model validation.

Data	Source	Resolution	Station name	Period
Observed runoff	Tibetan Hydrological Bureaus	Site, Monthly	Lhatse (LZ)	1971–2015
		Site, Monthly	Shigatse (RKZ)	1971–2015
		Site, Monthly	Lhasa (LS)	1971–2015
		Site, Monthly	Yangcun (YC)	1971–2015
		Site, Monthly	Nuxia (NX)	1971–2015
		Site, Monthly	Yigong (YG)	1981–2000
		Site, Monthly	Bomi (BM)	2004–2013
Glacier mass balance	Institute of Tibetan Plateau Research, Chinese Academy of Sciences (http://www.tpdac.ac.cn)	Site, Annual	Motuo (MT)	2015–2019
		Site, Annual	Gurenhekou	2005–2009
		Site, Annual	Parlung No.94	2006–2018
Glacier Inventory	The first Glacier Inventory of China (http://westdc.westgis.ac.cn/glacier)	–	–	1970s–1990s
Inventory	Randolph Glacier Inventory (RGI V6.0) (http://www.glims.org/RGI/)	–	–	2000s–2010s
Snow cover fraction	the Moderate Resolution Imaging Spectroradiometer (MODIS)10CM (https://nsidc.org/data)	0.05° × 0.05°, Monthly		2001–2019



Table 3. Trends in precipitation, temperature, total runoff, and three runoff components and their contributions to total runoff in the YZ basins for different periods. Asterisks indicate the 95% confidence level.

Basin		NX			NX-BXK			YZ		
Period		1971–	1971–	1998–	1971–	1971–	1998–	1971–	1971–	1998–
		2020	1997	2020	2020	1997	2020	2020	1997	2020
Precipitation (mm/10yr)		11.7 *	2.9	-6.9	-35.0 *	52	-16.4	2.1	8.3	-8.8
Temperature (°C/10yr)		0.4 *	0.2 *	0.3 *	0.1 *	0.1	0.3 *	0.3 *	0.2 *	0.3 *
Runoff (mm/10yr)	Total	9.4 *	1.1	-3.3	-21	48.1	-0.3	3.1	8.9	-2.7
	Glacier	1.1 *	0.6	0.7	6.0 *	0.1	16.1	2.0 *	0.1	3.9
	Snowmelt	-1	0.5	-3.4	-6	20.6 *	5.7	-1.9 *	4.6 *	-1.5
	Rainfall	9.4 *	0.9	-0.6	-22	27.6	-22.1	3.0	4.9	-5.0
Contribution (%/10yr)	Glacier	-0.1	-0.2	0.3	0.8 *	-0.7	1.2	0.3	-0.4	0.8
	Snowmelt	-1.1 *	0.3	-0.8	-0.1	0.9	0.3	-0.5 *	0.6	-0.3
	Rainfall	1.1 *	-0.1	0.6	-0.7 *	-0.3	-1.6 *	0.2	-0.2	-0.5



Table 4. Summary of relevant studies on simulated runoff component contributions in the YZ basin.

Basin	Runoff contribution (%)			Period	Method	Precipitation Data	References
	Glacier	Snowmelt	Rainfall				
Nuxia	11.6	23	65.4	1961–1999	VIC+DD	Corrected CMA data	Zhang et al. (2013)
	16	9	59	1998–2007	SPHY+DD	APHRODITE	Lutz et al. 2014
	15	27.3	57.7	1971–2000	VIC+DD	Corrected CMA data	Su et al. (2016)
	9.9	10.6	79.5	2003–2014	CREST	CGDPA, TMPA	Chen et al. (2017)
	5.5	23.1	71.4	1971–2010	VIC+DD	Interpolated CMA data	Zhao et al. (2019)
	13.9	23.8	62.3	1980–2000	VIC+DD	Reconstructed data	Sun and Su (2020)
	1.8	13.2	62.1	1985–2014	SPHY+DD	ERA5	Khanal et al. (2021)
	18.4	22	69.6	2001–2010	isoGSM	CMFD	Nan et al. (2021)
	3.5–7.2	16.6–22.3	—	1981–2019	WEB-DHM	Reconstructed data	Wang et al. (2021)
	13	24	63	1971–2020	VIC+DD	Corrected ERA5	This Study
	45.3	15.1	39.6	1980–2000	VIC+DD	Reconstructed data	Sun and Su (2020)
	5.7–8.2	7.2–7.8	—	1981–2019	WEB-DHM	Reconstructed data	Wang et al. (2021)
NX-BXX	19	21	60	1971–2020	VIC+DD	Corrected ERA5	This Study
YZ	32.7	18.4	48.9	1980–2000	VIC+DD	Reconstructed data	Sun and Su (2020)
	5.5	17.2	73.3	1981–2019	WEB-DHM	Reconstructed data	Wang et al. (2021)
	16	22	62	1971–2020	VIC+DD	Corrected ERA5	This Study

Note: VIC+DD=The Variable Infiltration Capacity (VIC) linked with a degree-day glacier melting model; SPHY+DD=The Spatial Processes in Hydrology (SPHY)

linked with a degree-day glacier melting model; CREST=Coupled Routing and Excess Storage model; isoGSM=Scripps global spectral model with water isotopes incorporated; WEB-DHM= Water and energy budget-based distributed hydrological model; CMFD= China Meteorological Forcing Dataset.